J|A|C|S
ARTICLES
Published on Web 06/18/2003

Photolytic Cleavage of 1-(2-Nitrophenyl)ethyl Ethers Involves Two Parallel Pathways and Product Release Is Rate-Limited by Decomposition of a Common Hemiacetal Intermediate

John E. T. Corrie,*,† Andreas Barth,§,# V. Ranjit N. Munasinghe,† David R. Trentham,† and Michael C. Hutter‡

Contribution from the National Institute for Medical Research, The Ridgeway, Mill Hill, London NW7 1AA, U.K., Institut für Biophysik, Johann Wolfgang Goethe-Universität, Theodor Stern Kai 7, Haus 74, D-60590 Frankfurt, Germany, and Max-Planck Institut für Biophysik, Kennedyallee 70, D-60590 Frankfurt, Germany

Received January 27, 2003; E-mail: jcorrie@nimr.mrc.ac.uk

Abstract: Time-resolved FTIR spectroscopic studies of the flash photolysis of several 1-(2-nitrophenyl)-ethyl ethers derived from aliphatic alcohols showed that a long-lived hemiacetal intermediate was formed during the reaction. Breakdown of this intermediate was rate-limiting for product release. One of these compounds (methyl 2-[1-(2-nitrophenyl)ethoxy]ethyl phosphate, **9**) was studied in detail by a combination of time-resolved FTIR and UV−vis spectroscopy. In addition, product studies confirmed clean photolytic decomposition to the expected alcohol, 2-hydroxyethyl methyl phosphate, and the 2-nitrosoacetophenone byproduct. At pH 7.0, 1 °C, the rate constant for product release was 0.11 s^{-1}, very much slower than the 5020 s^{-1} rate constant for decay of the photochemically generated *aci*-nitro intermediate (pH 7.0, 2 °C). Time-resolved UV−vis measurements showed that the hemiacetal intermediate is formed by two competing pathways, with fast (∼80% of the reaction flux) and slow (∼20% of the flux) components. Only the minor, slower path is responsible for the observed *aci*-nitro decay process. These competing reactions are interpreted with the aid of semiempirical PM3 calculations of reaction barriers. Furthermore, AMSOL calculations indicate that the pK_a of the nitronic acid isomer formed by photolysis is likely to determine partition into the alternate paths. These unusual results appear to be general for 1-(2-nitrophenyl)ethyl ethers and contrast with a related 2-nitrobenzyl ether that photolyzed without involvement of a long-lived hemiacetal.

Introduction

Flash photolytic release of bioactive molecular species by rapid cleavage of photolabile protecting groups from inactive precursors (colloquially termed caged compounds) is a valuable technique for time-resolved studies of biological processes.[1] The most common photochemistry in the field utilizes the well-known 2-nitrobenzyl rearrangement, in which a nitrobenzyl group, or substituted version thereof, is converted to a 2-nitrosoarylcarbonyl compound, with release of the species to which it was attached. In the archetypal example of caged ATP **1**, the dark reactions after the photolytic event have been interpreted as in Scheme 1, with decay of the *aci*-nitro intermediate **2** having been shown to be the rate-limiting step for product release.[2,3] The reaction proceeds via rapid equilibration of the conjugate acid of **2** with the bicyclic species **3**, collapse of which generates the final products, namely, ATP

Scheme 1

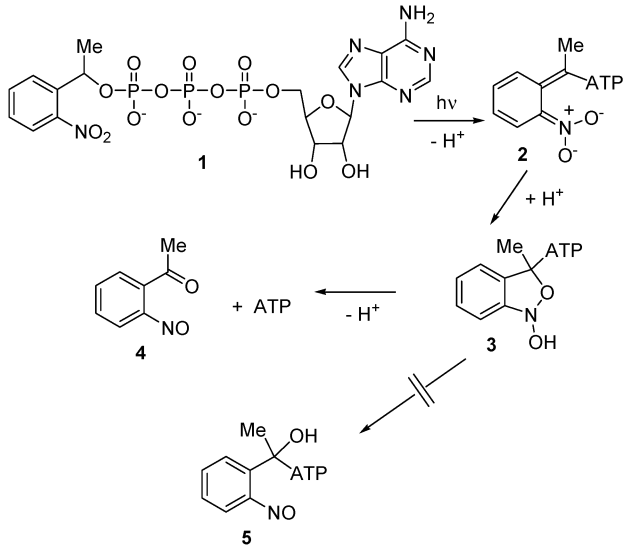

† National Institute for Medical Research.
§ Johann Wolfgang Goethe-Universität.
# Present address: Department of Biochemistry and Biophysics, Arrhenius Laboratories for Natural Sciences, Stockholm University, SE-106 91 Stockholm, Sweden.
‡ Max-Planck Institut für Biophysik.

(1) (a) Corrie, J. E. T.; Trentham, D. R. In *Bioorganic Photochemistry*; Morrison, H., Ed.; Wiley: New York, 1993; Vol. 2, pp 243−305. (b) Adams, S. R.; Tsien, R. Y. *Annu. Rev. Physiol.* **1993**, *55*, 755. (c) Kaplan, J. H. *Annu. Rev. Physiol.* **1990**, *52*, 897. (d) Marriott, G., Ed. *Methods in Enzymology*; Academic Press: San Diego, 1998; Vol. 291. (e) Pelliccioli, A. P.; Wirz, J. *Photochem. Photobiol. Sci.* **2002**, *1*, 441.

10.1021/ja034354c CCC: $25.00

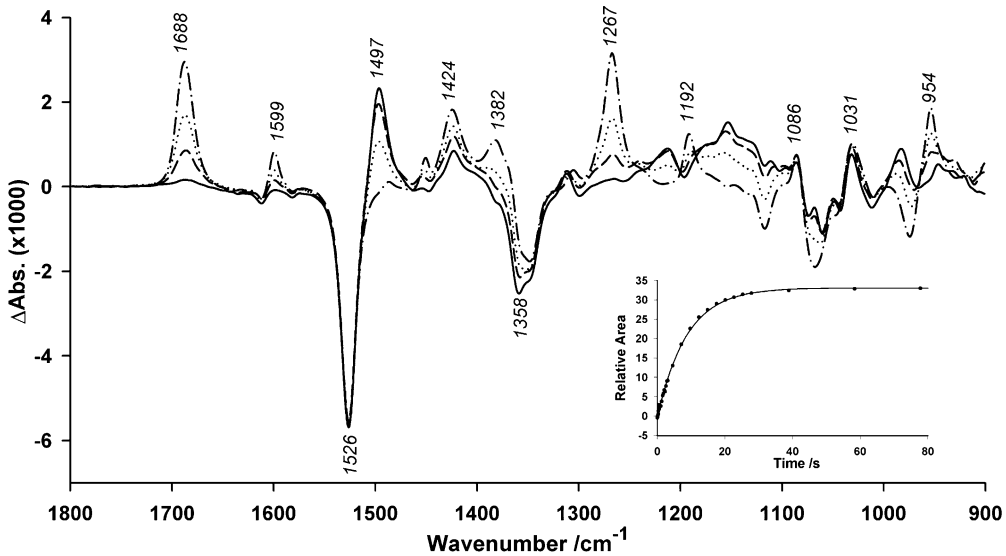

Figure 1. IR difference spectra for photolysis of **9** at pH 7.0, 1 °C in 200 mM MOPS buffer. The traces represent spectra averaged in the following time windows after the light flash: (—) 0.01−1.16 s, (- - -) 2.5−3.2 s, (···) 3.2−11.0 s, (— · —) 68.1−126.4 s. The inset shows a single-exponential fit to the integrated area of the 1688 cm^{-1} peak with respect to time.

and the nitrosoketone **4**. The protonation state shown for **3** takes account of recent studies,[4] so differs from a previous proposal[2] in which **3** was suggested to be formed as its conjugate base, i.e., by cyclization of the *aci*-nitro anion **2** without uptake of a proton. In the case of caged ATP, an alternative collapse of **3** via a further hemiacetal species **5** was previously excluded, at least insofar that the hemiacetal did not accumulate to a measurable extent.[2] In light of the results reported below, **5** may in fact be in the pathway, but previous work[2] implies that it would break down immediately.

As part of our use of time-resolved IR spectroscopy initiated by flash photolysis to elucidate dark reactions in a range of 2-nitrobenzyl photocleavage processes,[3] we studied **6**, the 1-(2-nitrophenyl)ethyl ether of glycolic acid, because we had observed photodecarboxylation of several related compounds (A. Barth and J. E. T. Corrie, unpublished data). In fact, time-resolved IR difference spectra recorded upon photolysis of **6** showed that photodecarboxylation was only a very minor process for this compound. Of much greater interest in the spectrum were changes of several strong transient bands that appeared to be consistent with the formation and subsequent decay of a relatively long-lived hemiacetal intermediate. At pH 7, breakdown of this intermediate to release the caged species (in this case the glycolate anion) was 4 orders of magnitude slower than decay of the upstream *aci*-nitro intermediate. This observation was particularly significant, as *aci*-nitro decay rates have often been used to estimate product release rates, an assumption based on the case of caged ATP, where product release has unequivocally been shown to be synchronous with *aci*-nitro decay.[2,3] Whether an *aci*-nitro decay rate necessarily provides a reliable measure of the rate of product release is an issue of concern in this field.[1d,5] In the case of a caged choline **7**, an ether derivative of the same type as **6**, rapid decay of the *aci*-nitro intermediate formed on photolysis has been taken as evidence for rapid release of choline. The result was proposed to make **7** and its arsenic analogue suitable precursors for time-resolved X-ray crystallographic studies.[6]

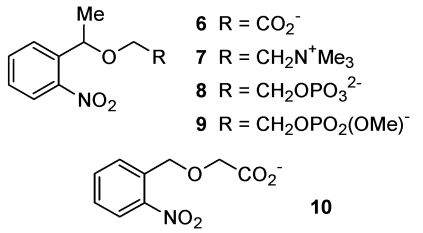

Following the initial observations on **6**, we studied the photolysis of ethers **7**−**9** and found that all had similar behavior, with decay of a putative hemiacetal intermediate being the rate-determining step for release of the various alcohol products. Of these compounds, **9** was investigated in greatest detail, as it was a readily accessed water-soluble species that was expected to avoid unwanted side reactions such as the minor decarboxylation seen for **6**. The compounds **6**−**8** are discussed only where they give rise to specific points, particularly in the rate of breakdown of the hemiacetal intermediate. In contrast to these results for **6**−**9**, the related ether **10** that lacks the benzylic methyl substituent photolyzed with no evidence of a long-lived intermediate. These results and their implications are described below, together with results of semiempirical molecular orbital calculations that shed light on the mechanistic processes involved.

Results and Discussion

It was evident from time-resolved IR difference spectra for flash photolysis of **9** at pH 7.0, 1 °C (Figure 1) that slow processes were involved in the overall reaction. In these spectra, negative bands represent absorption by species that disappear from the solution as a result of photolysis, while positive bands

(2) Walker, J. W.; Reid, G. P.; McCray, J. A.; Trentham, D. R. *J. Am. Chem. Soc.* **1988**, *110*, 7170.
(3) Barth, A.; Corrie, J. E. T.; Gradwell, M. J.; Maeda, Y.; Mäntele, W.; Meier, T.; Trentham, D. R. *J. Am. Chem. Soc.* **1997**, *119*, 4149.
(4) (a) Il'ichev, Y. V.; Wirz, J. *J. Phys. Chem. A* **2000**, *104*, 7856. (b) Schwörer, M.; Wirz, J. *Helv. Chim. Acta* **2001**, *84*, 1441.
(5) McCray, J. A.; Trentham, D. R. *Annu. Rev. Biophys. Biophys. Chem.* **1989**, *18*, 239.
(6) (a) Peng, L.; Goeldner, M. *J. Org. Chem.* **1996**, *61*, 185. (b) Peng, L.; Nachon, F.; Wirz, J.; Goeldner, M. *Angew. Chem., Int. Ed.* **1998**, *37*, 2691.

arise from species produced in the reaction. Notably, the spectrum recorded in the 0.01−1.16 s time window after photolysis showed minimal carbonyl absorption but had an intense band at 1497 cm^{-1} that was assigned to a nitroso monomer.[3,7] A carbonyl band gradually appeared at 1688 cm^{-1} and reached its maximum intensity over the following ∼100 s, while the nitroso monomer band decayed to zero on the same time scale and was replaced by bands characteristic of nitroso dimers at 1424 and 1382 cm^{-1} (*cis*-dimer) and 1267 cm^{-1} (*trans*-dimer).[3,7]

These spectroscopic features, particularly the strong nitroso monomer band and the absence of a carbonyl band in spectra taken soon after the flash, are most readily compatible with the hemiacetal **11** being a relatively long-lived intermediate. Breakdown of **11** would release as products the alcohol **12** and nitrosoketone **4**, the latter giving rise to the observed carbonyl band. Decay rates of the *aci*-nitro intermediate in photolysis of **9** (and the related ethers **6**−**8**) were always too fast in the pH range 6−10 to allow this species to be seen in our FTIR spectra, in which **11** was the first observable intermediate for these compounds. This contrasts with previous results for caged ATP, where decay of the *aci*-nitro intermediate was much slower.[3,8] To the best of our knowledge, the only related report of a verified "stable" hemiacetal-like intermediate from photolysis of 2-nitrobenzyl compounds is from *N*-(2-nitrobenzyl)-1-naphthalenecarboxamide, where the aminol **13** was reported as an isolable compound that underwent slow decomposition to 1-naphthalenecarboxamide and 2-nitrosobenzaldehyde.[9]

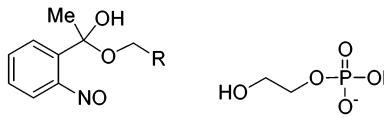

11

12

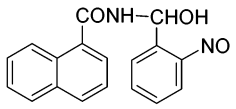

13

Time-resolved FTIR measurements for **9** over the pH range 6−10 gave spectra qualitatively similar to those recorded at pH 7 (Figure 1), except that the rates of change of various bands were pH-dependent. Rate constants for the formation of ketone **4**, and by inference for release of the alcohol product, were determined by integration of the area of the carbonyl band as a function of time (Table 1). Formation of the carbonyl band became faster at higher pH values; that is, breakdown of the hemiacetal intermediate **11** was base-catalyzed (see below). Similar integration of the nitroso monomer band gave information on its rate of disappearance as a consequence of dimerization (Table 1). This process at pH 6 and 7 had the same rate constant (within experimental error) as that for carbonyl formation; that is, the dimerization was rate-limited by decomposition of the hemiacetal **11**. The kinetics became more complex at higher pH values and lagged behind the carbonyl formation. The data suggest that the nitroso group of **11** does not undergo significant dimerization, presumably because of hindrance by the bulky *ortho*-substituent; so dimer formation proceeds only as the nitrosoketone **4** is released. However, the kinetics of nitroso dimerization were not the main focus of this work and were not studied in detail.

Table 1. Rate Constants for Processes Initiated by Flash Photolysis of **9**

	rate constant (s^{-1})		
pH	*aci*-nitro decay[a] (406 nm)	carbonyl formation[b] (1688 cm^{-1})	nitroso dimerization[b,c] (1497 cm^{-1})
6.0	n.d.	0.01	0.02
7.0	5020	0.11	0.12
7.5	2600	n.d.	n.d.
8.0	1490	0.79	$t_{1/2}$ 1.9 s
8.5	650	n.d.	n.d.
9.0	225	5	$t_{1/2}$ 1.0 s
9.5	246	n.d.	n.d.
10.0	190	>50	$t_{1/2}$ 1.6 s
10.5	138	n.d.	n.d.

[a] Measured at 2 °C in 20 mM MES, MOPS, EPPS, CHES, or CAPS buffers plus 150 mM NaCl (see Experimental Section for details). [b] Measured at 1 °C in 200 mM MES, MOPS, EPPS, CHES, or CAPS buffers (see Experimental Section for details). [c] Data at pH 8, 9, and 10 did not fit to single exponentials and are expressed as half-times for the overall amplitude change.

To substantiate the formation of **11** and establish an overall reaction mechanism, time-resolved UV and visible recordings initiated by flash photolysis of **9** were made. Recordings of the *aci*-nitro decay at 406 nm over the pH range 7.0−10.5 and at 2 °C (Table 1) showed clean, single-exponential processes in all cases (e.g., Figure 2c), and the amplitude of the signal was constant across this pH range. The rate constant at pH 7.0, 2 °C (5020 s^{-1}) is consistent with the value of 6300 s^{-1} at pH 7.2, 20 °C reported for **7** by Peng and Goeldner[6a] (see below for comment on the buffer dependence of this rate constant). As with other 1-(2-nitrophenyl)ethyl derivatives,[1a,2] the *aci*-nitro decay became slower as the pH increased.

Further measurements to monitor the kinetics of nitroso monomer formation (at 740 nm) and at 577 nm in the presence of a pH indicator (Cresol Purple) to follow proton transients were made at pH 8.5, where the rate constants were in a convenient range. At 740 nm, we had expected to observe an exponential increase in absorbance at a rate that mirrored decay of the *aci*-nitro absorbance at 406 nm, as reported for photolysis of caged ATP **1**.[2] In practice, the 740 nm data for **9** upon flash photolysis (Figure 2a) showed a large step increase in absorption (i.e., a rate constant $>10^5$ s^{-1}, which was the resolution limit of our apparatus) followed by an exponential increase with rate constant 650 s^{-1}, which matched the *aci*-nitro decay at this pH value (Table 1). The slow phase comprised ∼20% of the total amplitude.

Measurements of proton transients following flash photolysis were made in weakly buffered solutions for **9** and caged ATP at pH 8.5, 2 °C (Figure 2b) by a method previously described.[2,10] As expected at this pH, caged ATP showed only a rapid ($>10^5$ s^{-1}) decrease in pH from the proton released during ionization of the initially formed nitronic acid (Scheme 1). In contrast, **9** showed rapid proton release, with the amplitude of the initial acidification step being ∼15% of that for caged ATP under the same conditions, followed by an exponential return to the initial

(7) Colthup, N. B.; Daly, L. H.; Wiberley, S. E. *Introduction to Infrared and Raman Spectroscopy*, 3rd ed.; Academic Press: San Diego, 1990.
(8) Barth, A.; Hauser, K.; Mäntele, W.; Corrie, J. E. T.; Trentham, D. R. *J. Am. Chem. Soc.* **1995**, *117*, 10311.
(9) Peyser, J. R.; Fletchner, T. W. *J. Org. Chem.* **1987**, *52*, 4645.
(10) Papageorgiou, G.; Corrie, J. E. T. *Tetrahedron* **1997**, *53*, 3917.

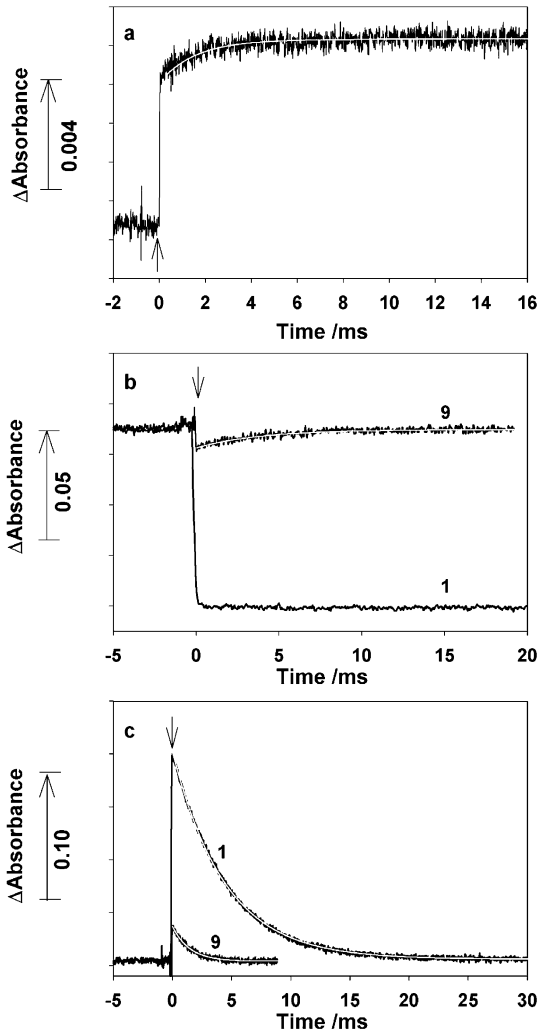

Figure 2. Transients for flash photolysis of caged ATP **1** and the ether **9**. (a) Nitroso monomer formation: measured at 740 nm for a 3 mM solution of **9** in 20 mM EPPS, 150 mM NaCl, pH 8.5 at 2 °C. (b) Proton transients: measured at 577 nm in the presence of Cresol Purple indicator for 0.5 mM solutions of **1** or **9** in 1 mM EPPS, 150 mM NaCl, pH 8.5, 2 °C. (c) *aci*-Nitro transients: measured at 406 nm, 2 °C for 0.5 mM solutions of **1** (226 s^{-1} in 25 mM MES, pH 6.5) or **9** (688 s^{-1} in 25 mM EPPS, pH 8.5). The arrows on each panel indicate the time of the laser flash. Perturbations in the records that start ~0.8 ms prior to the laser flash arise from the flash lamp that initiates the laser pulse. The clear lines superimposed on the traces in each panel represent single-exponential fits to relevant sections of the data.

pH (rate constant 280 s^{-1}). Essentially the same rate constant (250 s^{-1}) was measured for the *aci*-nitro decay of **9** under these solution conditions but in the absence of the pH indicator (data not shown). It should be noted that there are significant buffer effects on the kinetics of this *aci*-nitro decay. Measurements at pH 8.5, 2 °C in four solutions that were used in different parts of this work (25 mM Na EPPS, 20 mM Na EPPS + 150 mM NaCl, 1 mM Na EPPS + 150 mM NaCl, and 10 mM Na pyrophosphate + 100 mM NaCl) gave rate constants of 688, 650, 250, and 1040 s^{-1}, respectively. These differences appear to be mediated more by the particular buffer conditions than by nonspecific ionic strength effects (cf. ref 5 for an example of the ionic strength dependence for caged ATP) but were not investigated further.

Return of the pH to its initial value in the photolytic reaction of **9** was consistent with FTIR spectra recorded in a carboxylate

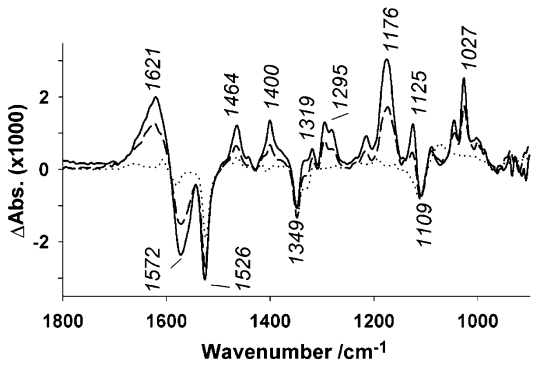

Figure 3. IR difference spectra for photolysis of **10** at pH 8.5, 1 °C in 200 mM Bicine buffer. The traces represent spectra averaged in the following time windows after the light flash: (—) 0.01−0.185 s, (- - -) 0.196−0.51 s, (···) 3.2−29.0 s.

buffer (Bicine, pH 8.5) that showed no change of buffer protonation state during or after the photolytic reaction (data not shown). In contrast, similar FTIR spectra recorded for compounds that undergo slower transient or permanent proton release upon photolysis show large difference bands at 1621 and 1572 cm^{-1} for Bicine protonation (for examples of transient and permanent changes, see Figure 3 and ref 11, respectively). The proton transient recorded for **9** in the indicator study above is too rapid to observe in our FTIR spectra. The absence of a net pH change upon photolysis of **9** is expected, since the reaction stoichiometry predicts that the proton released upon ionization of the photolytically formed nitronic acid ultimately returns to the product alcohol **12**. However, the small amplitude of the pH transient observed during the photolysis in comparison with that for caged ATP **1** (Figure 2b) is noteworthy, since the two compounds have similar quantum yields (0.63 for caged ATP[2] and 0.54 measured for **9**; see Supporting Information) and an identical near-UV chromophore. Despite this similarity of quantum yields, the amplitude of the 406 nm *aci*-nitro transient for **9** was ~18% of that for caged ATP (Figure 2c), close to the relative amplitudes of the proton transients from the two compounds (Figure 2b). These 406 nm measurements were made at different pH values for the two compounds to bring their *aci*-nitro decay processes into a similar time frame (see caption to Figure 2c).

The 740 nm measurement described above gives direct evidence of processes occurring on two very different time scales, with a fast process accounting for the majority of the reaction flux. The relative amplitudes of the comparative measurements of proton stoichiometry and *aci*-nitro decay for caged ATP and **9** agree well with those of the fast and slow phases of the 740 nm data. In light of these congruent but unexpected results, we were concerned that formation of product(s) other than those of the "normal" 2-nitrobenzyl photochemistry, as exemplified in Scheme 1, might be responsible for the large-amplitude fast phase of the 740 nm transient recorded for the photoreaction of **9**. Evidence that this was not the case came from two independent sources. First, clean formation of the expected product (2-hydroxyethyl methyl phosphate **12**) was confirmed by ^{1}H NMR spectroscopy of a partially photolyzed solution of **9** (~40% conversion). This NMR spectrum was compared with that of a solution that contained a 1:1 mixture of unphotolyzed **9** and authentic **12**.

(11) Barth, A.; Corrie, J. E. T. *Biophys. J.* **2002**, *83*, 2864.

Table 2. Rate Constants for Decomposition of the Hemiacetal Intermediate **11** Formed upon Photolysis of **6**−**9**

	rate constant (s^{-1})[a]			
pH	**6**	**7**	**8**	**9**
6.0	0.11	n.d.	0.26	0.012
7.0	0.21	1.1	0.35	0.11
8.0	0.90	n.d.	0.45	0.79
9.0	7.0	n.d.	0.70	5.0

[a] Measured at 1 °C in 200 mM MES, MOPS, EPPS, or CHES buffers by monitoring the formation of the carbonyl band at 1688 cm^{-1} (see Experimental Section for details).

The latter spectrum showed characteristic, clearly resolved signals for each species, so was appropriate for this product analysis. The ^{1}H NMR spectrum of the partially photolyzed sample of **9** essentially showed signals only for the starting material and **12** together with the normal byproduct, 2-nitrosoacetophenone **4** (see Supporting Information, Figures S1 and S2). Signals for the latter were weak, probably because of substantial precipitation of this water-insoluble compound between the time of photolysis and recording the NMR spectrum. Stronger evidence for predominant formation of **4** (in this case from compound **6**, which had a biphasic 740 nm transient upon photolysis very similar to that of **9**) came from FTIR spectroscopy at pH 6, 35 °C in the presence of dithiothreitol. We have previously described the sequence of reactions and consequent IR spectroscopic changes of **4** under these conditions when generated by photolysis of caged ATP (i.e., initial rapid formation of 2-hydroxylaminoacetophenone, followed more slowly by dehydration to 3-methylanthranil).[3] Exactly the same sequence of spectra was observed upon photolysis of **6** (data not shown). Thus the product studies indicate that **9** undergoes photolysis to the expected products **4** and **12** with no evidence of additional products being formed and indicate that both the fast and slow 740 nm transients represent processes on pathways to **4** and **12**.

Compounds **6**−**8** each gave FTIR spectra upon photolysis with features similar to those in Figure 1, suggesting that the unusual reactivity of **9** is common to 1-(2-nitrophenyl)ethyl ethers of aliphatic alcohols. As mentioned above, **6** had the same biphasic growth of absorption at 740 nm, indicating that a dual reaction pathway also operates for that compound, and by inference for **7** and **8** as well. The main difference detected among the various compounds was in the rate constants for release of the respective alcohol products. These data (Table 2) show that the rates of breakdown of the hemiacetal intermediates are modulated by the terminal substituent on the ethoxy group and are compatible with base-catalyzed breakdown of a hemiacetal intermediate. The most notable variation is for **8**, where rates at pH 6 and 7 were similar to those for **6** and **9**. However by pH 8, where the terminal dibasic phosphate is fully ionized, the rate began to slow and was less strongly catalyzed by increasing alkalinity of the solution.

Scheme 2 shows a branched mechanism for the dark reactions after photolysis to interpret these time-resolved IR and UV−vis data for **9** and related ethers. In its final step, it shows base-catalyzed breakdown of the hemiacetal **11** in accord with the data of Table 1. Base catalysis is in line with studies by McClelland et al.[12] on hydrolysis of hemiacetals of acetophenone

Scheme 2. Proposed Two-Path Mechanism for the Dark Reactions Subsequent to Flash Photolysis of **6**−**9**[a]

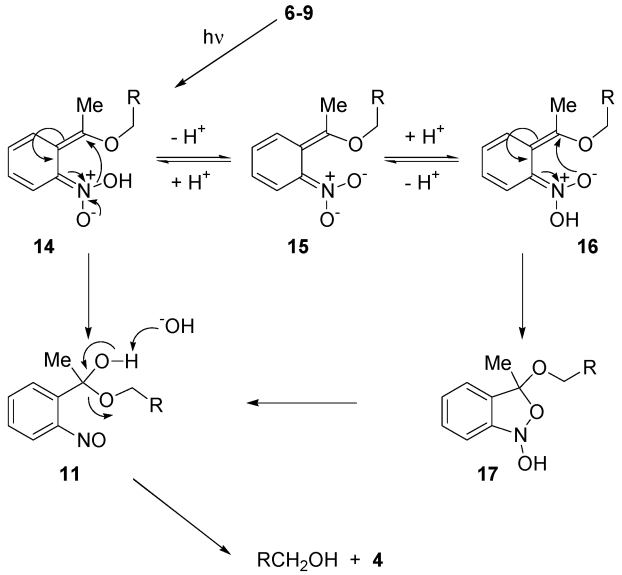

[a] The arrows representing electron movements on structure **14** refer to its direct route to **11**, while those on **16** refer to the conversion into **17**.

and its substituted analogues. The proposed partition for decay of the nitronic acid **14**, which is generally regarded as the product of the photolytic step in 2-nitrobenzyl photochemistry, is introduced to rationalize biphasic formation of the nitroso monomer (Figure 2a) and the low amplitudes of the proton and *aci*-nitro transients compared with corresponding signals from caged ATP (Figures 2b and 2c, respectively). The minor pathway for **9** proceeds via **15** and equilibration with the isomeric nitronic acid **16**, which further undergoes conversion to the bicyclic species **17** and subsequent breakdown to the hemiacetal **11**. This path accounts for 15−20% of the reaction flux for **9**, as shown by the amplitudes of the *aci*-nitro and pH transients in comparison with those of caged ATP and by the amplitude of the slow phase of nitroso formation. This minor path, at least up to **17**, is analogous to the well-established mechanism shown in Scheme 1 for caged ATP and represents the exponential processes shown for **9** in Figure 2a−c. The major pathway of Scheme 2 is suggested to proceed by an electrocyclic rearrangement of **14** to **11** and is represented by the sub-millisecond transient in Figure 2a, so comprises ∼80% of the reaction flux. Because ionization of the initial nitronic acid that leads into the "normal" pathway (i.e., as for caged ATP) via **15** is rapid (within the time scale of the laser flash for solutions containing buffer salts[4b]), entry to the competing, major pathway must necessarily be on the same time scale.

Remarkably, the unsubstituted 2-nitrobenzyl ether **10**, i.e., the analogue of **6** that lacks the α-methyl group, had quite different reactivity from that of **6**−**9**. Its *aci*-nitro decay rate (515 s^{-1} at pH 7.0, 20 °C) was much slower than for its methyl-substituted analogue **6** (5690 s^{-1} at pH 7.5, 17 °C). Measurement at 740 nm to monitor nitroso formation showed a single-exponential rise in absorption with a rate constant of 590 s^{-1} (pH 7, 20 °C; data not shown), comparable to that of the *aci*-nitro decay process. This trace had no evidence of a sub-millisecond component as seen for **9** (Figure 2a). The slower decay kinetics in this case made it possible to observe the *aci*-nitro intermediate in the time-resolved IR spectrum (Figure 3;

(12) McClelland, R. A.; Engell, K. M.; Larsen, T. S.; Sørensen, P. S. *J. Chem. Soc., Perkin Trans. 2* **1994**, 2199.

Bicine, pH 8.5, 1 °C). Positive bands at 1464, 1319, and 1176 cm^{-1} are close to positions of bands at 1465, 1330, and 1179 cm^{-1} that were assigned in the *aci*-nitro spectrum of caged ATP to vibrations involving the nitronate group,[8] and a sharp band at 1027 cm^{-1} probably arises from the enol ether moiety. The spectrum also showed strong difference bands for buffer protonation (negative at 1572 cm^{-1} and positive at 1621 cm^{-1}) that return to baseline as this intermediate decays to the final products; that is, the reaction has no net proton release since, as discussed above for the related compound **9**, the proton initially released from the benzylic position is eventually taken up on the alcohol product.

Two further points are relevant to the IR spectra observed upon photolysis of **10**. First, apart from the negative bands that correspond to disappearance of the original nitro group, the spectrum at the end of the dark processes is almost featureless (Figure 3), in contrast to the corresponding final spectrum for **9**. The lack of significant IR absorptions in this case can be attributed to hydration of the 2-nitrosobenzaldehyde byproduct. Electron-withdrawing substituents are known to promote hydration of aromatic aldehydes,[13] and in the present case hydration would additionally be favored by formation of the cyclic tautomer **18**. It therefore seems probable that 2-nitrosobenzaldehyde undergoes hydration as it is formed, so only the weakly absorbing tautomer **18** is present. Clean release of glycolate on photolysis of **10** was inferred from previous data for a 2-nitrobenzyl ether [2-*O*-(2-nitrobenzyl)-D-glucose **19**], where stoichiometric release of D-glucose upon photolysis was confirmed by an enzymatic assay.[14] Time-resolved IR spectra for **19** upon flash photolysis also showed an *aci*-nitro intermediate, followed by reversion to a near-featureless spectrum (data not shown), as observed for **10**. The second issue in the photolysis of **10** is the absence of any evidence for a hemiacetal intermediate. Rates for breakdown of hemiacetals derived from benzaldehydes and acetophenones are dominated by hydroxide ion catalysis at alkaline pH values, and the second-order rate constants for hydroxide ion catalysis are an order of magnitude lower for aldehyde-derived hemiacetals than those for those derived from ketones.[12,15,16] Hence if a hemiacetal intermediate analogous to **11** were formed in the photolysis of **10** at pH 8.5, it should have had a lifetime of at least several seconds, substantially longer than the observed lifetime of the *aci*-nitro intermediate from **10** (~0.4 s at 1 °C), and therefore should have been observable in our FTIR spectra, inter alia by the presence of a strong nitroso monomer band. The absence of such a band thus excludes a hemiacetal intermediate and **10** appears exclusively to undergo photocleavage by a "normal" pathway analogous to that shown in Scheme 1, i.e., direct collapse of a bicyclic intermediate equivalent to **3** to yield the end products. A referee has drawn our attention to unpublished work briefly described in a review article,[1e] where it is indicated that photolysis of 2-nitrobenzyl methyl ether in nonaqueous or aqueous solvents gave evidence of a hemiacetal intermediate. This contrasts with the results described here for the 2-nitrobenzyl ether **10** in purely aqueous conditions. Full publication of these unpublished data will clearly be of interest, but at present insufficient information is available to permit detailed comparisons with our work.

Table 3. PM3 Computed Reaction Barriers (kJ mol^{-1}) for Processes in Scheme 2

	reaction step		
compound[a]	**14** → **11**	**16** → **17**	**17** → **11**[b]
6	81.6	62.4	130.2
6 + H^+	118.5	102.2	136.9
7	113.9	113.9	147.0
7 + Cl^-	112.2	105.9	135.7
8 + H^+	113.5	98.0	131.1
8 + $2H^+$	118.9	102.2	134.4
9	110.1	93.8	136.1
9 + H^+	119.7	110.6	132.3
10	98.4	93.0	134.8
10 + H^+	119.7	106.3	137.3
20	118.5	105.1	142.4
21	122.7	104.3	139.0

[a] Compounds **6**, **9**, and **10** were treated as the monoanions or their conjugate acids, compound **8** as its mono- or diprotonated form, and compound **7** as the free cation or as an ion pair with a chloride ion. [b] Via water-mediated proton exchange. The reaction barrier is expected to be considerably lower in water.

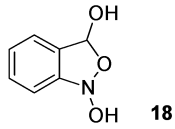

18

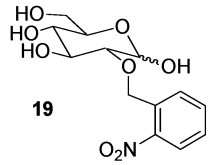

19

To obtain some insight into the unusual reactivity shown by **6**−**9** in comparison with the photocleavage of **10**, we performed gas-phase semiempirical PM3 calculations[17] for a number of the steps shown in Scheme 2. The PM3 method was chosen, as it yields the best results for organophosphorus and nitro compounds among the MNDO-type Hamiltonians.[18] The suitability of the method for **6**−**10** was also checked where possible by comparison of our results with previous high-level calculations on the isomerization of 2-nitrotoluene to 2-nitrosobenzyl alcohol[4a] [B3LYP/6-311+G(2d,p)] or on the same isomerization and that of 2-nitrobenzyl methyl ether[19] [B3PW91/6-31G(d)] (see below).

Reaction barriers were calculated for the steps **14** → **11**, **16** → **17**, and **17** → **11** for each of compounds **6**−**9**, nitrobenzyloxy compound **10**, and model alcohols **20** and **21**, which are uncharged analogues of **6**−**10** (Table 3). For the ionic compounds, the calculations were performed in different ionization states, as shown in Table 3, to establish whether the charged side chains significantly influenced the calculated reaction barriers. Several points stand out among these data. With the exception of the data for **6** in its anionic form, the barriers calculated over the range of compounds did not vary greatly within each process, and values for the uncharged compounds **20** and **21** were similar to those for the ionic species. Second, the barriers calculated for the direct conversion of **14** to **11** were consistently higher than for the step of the competing pathway that involves cyclization of **16** to the benzisoxazoline **17**, but in no case by >19.3 kJ mol^{-1}. The relatively close magnitude of these calculated barriers leaves open a reasonable possibility that the two pathways could operate in competition (see below),

(13) McClelland, R. A.; Coe, M. *J. Am. Chem. Soc.* **1983**, *105*, 2718.
(14) Corrie, J. E. T. *J. Chem. Soc., Perkin Trans. 1* **1993**, 2161.
(15) Cox, B. G.; Kresge, A. J.; Sørensen, P. E. *Acta Chem. Scand.* **1988**, *A42*, 202.
(16) Engell, K. E.; McClelland, R. A.; Sørensen, P. E. *Can. J. Chem.* **1999**, *77*, 978.
(17) Stewart, J. J. P. *J. Comput. Chem.* **1989**, *10*, 209.
(18) Stewart, J. J. P. *J. Comput. Chem.* **1989**, *10*, 221.
(19) Dunkin, I. R.; Gebicki, J.; Kiszka, M.; Sanín-Leira, D. *J. Chem. Soc., Perkin Trans. 2* **2001**, 1414.

especially as the photochemically generated **14** is probably formed in a vibrationally excited state that would facilitate crossing of activation barriers. No pathway with a barrier that could reasonably be crossed was found for a direct route from the initial nitronic acid **14** to the bicyclic intermediate **17**. Such a step would have provided an alternative product-directed exit from **14**, but its inaccessibility appears to leave only the one-step **14** → **11** route available.

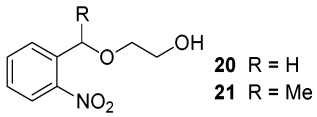

20 R = H
21 R = Me

Our measurements of *aci*-nitro and pH transients have confirmed the presence of **15** as an intermediate between **14** and **16**, and direct isomerization of **14** to **16** by rotation about the C═N bond has been excluded by previous workers, either by comparison with experimental values of ∼210 kJ mol^{-1} for oxime ethers[4a] or from a calculated[19] barrier of 157 kJ mol^{-1}. Our calculations yielded a barrier >124 kJ mol^{-1} for this rotation in the species **14** derived from **6**−**9**. For an alternative conversion of **14** to **16** via direct proton shift between the two oxygens of the *aci*-nitro group (without participation of a water molecule), the activation barriers computed by density functional calculations are in the range 85−95 kJ mol^{-1} for the unsubstituted nitronic acid derived from 2-nitrotoluene,[19] while calculated barriers for our substituted molecules are ∼142 kJ mol^{-1}. This difference is not surprising, given the different basis sets used. The reaction would involve strong localization of positive charge on the shifted proton, so it can be expected that high-level methods, which employ substantial basis sets for hydrogen, will yield lower activation barriers than MNDO-type methods that use only a minimal basis set. Furthermore, inclusion of a single water molecule to mediate the shift of this proton is computed in our PM3 calculations to lower the activation barrier by at least 29 kJ mol^{-1} compared to the direct shift. The presence of additional water molecules in bulk solution that are within hydrogen bonding distance of the transiently formed H_3O^+ should lower the activation barrier for water-mediated proton exchange even further. A previous computational study of such effects on proton transfer barriers showed that the barrier for proton transfer from imidazole to water is lowered by 84 kJ mol^{-1} in the presence of two ligand water molecules.[20] Taking this solvation effect into account, water-mediated proton exchange via the anion **15** can be assumed to be the most likely path between the nitronic acid isomers **14** and **16**, with an activation barrier of only a few kJ mol^{-1}.

As foreshadowed in the Introduction, direct cyclization of the *aci*-nitro anion **15** to the anion of **17** can be excluded. Il'ichev and Wirz[4a] found this step in the case of the reaction for 2-nitrotoluene to have an activation barrier in the region of 167 kJ mol^{-1} and to be strongly endothermic. In contrast, they reported that cyclization of the neutral form (corresponding to the process **16** → **17**) was exothermic, with an activation barrier in the range 77−102 kJ mol^{-1}. Dunkin et al.[19] calculated a barrier of 59 kJ mol^{-1} for the corresponding step in the reaction of 2-nitrobenzyl methyl ether. These calculations agree reasonably with our calculated barriers of ∼105 kJ mol^{-1} for the process (Table 3), which we calculated also to be exothermic by ∼105 kJ mol^{-1}.

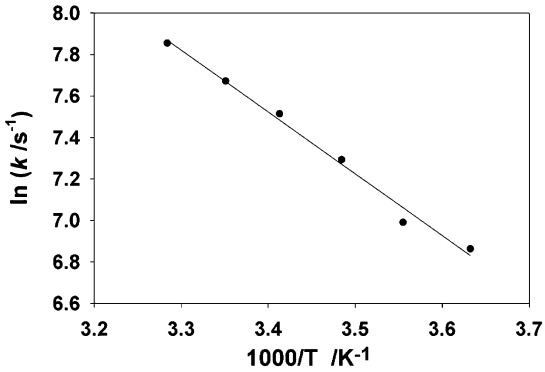

Figure 4. Arrhenius plot of the kinetics of *aci*-nitro decay following flash photolysis of **9** at pH 8.5.

Finally, barriers calculated for ring opening of **17** to give hemiacetal **11** were fairly consistent over the range of compounds. The calculation was done for a water-mediated pathway, and the barriers reported in Table 3 represent the rate-limiting step of initial transfer of the N−OH proton to a water molecule. For the subsequent shift of the proton to the endocyclic oxygen of the benzisoxazoline, the computed barrier was only a few kJ mol^{-1}. As discussed above, the barrier for the initial proton transfer would be substantially lower in bulk water than for the gas-phase calculation, so the actual barrier in solution for the process **17** → **11** is probably comparable to that for cyclization of **16**. Furthermore, base catalysis of this process is likely to operate under the conditions studied here. It is relevant in this context that benzisoxazoline intermediates similar to **17** have not to our knowledge been observed to accumulate in photolytic reactions of any 2-nitrobenzyl system in aqueous solution.

The extent of the reduction in the calculated activation barriers when reaction takes place in bulk solvent was investigated for decay of the *aci*-nitro intermediate **15** generated upon photolysis of **9**, i.e., the step presumed to operate via the pathway **15** ⇌ **16** → **17**, which is considered from the experimental data above to represent the minor pathway for overall product formation. The temperature dependence of the process was measured over the range 2.3−31.5 °C for a solution buffered at pH 8.5 by 10 mM sodium pyrophosphate. This salt was used, as phosphates have a low heat of ionization.[21] The Arrhenius plot for these data (Figure 4) gave an activation energy of 24.8 kJ mol^{-1}, which is presumably for the highest barrier in the steps between **15** and **11**. This implies that the rate-determining step in the overall process is not opening of the bicyclic intermediate **17** to the hemiacetal **11**, since the measured rate constants of the slow phase of nitroso formation (that corresponds to **17** → **11**) and of *aci*-nitro decay (that corresponds to overall **15** → **17**) are identical. The measured 24.8 kJ mol^{-1} barrier for the overall decay of the *aci*-nitro anion **15** is therefore in one of the steps between **15** and **17**, but in this kinetically complex process we do not attempt to assign it to an individual step. The activation energy measured in solution is 63−126 kJ mol^{-1} lower than the calculated gas-phase values in Table 3 for the steps **16** → **17** and **17** → **11** and is substantially below the 62 kJ mol^{-1} previously measured for the *aci*-nitro decay process of caged

(20) Lill, M. A.; Hutter, M. C.; Helms, V. *J. Phys. Chem. A* **2000**, *104*, 8283.

(21) Edsall, J. T.; Gutfreund, H. *Biothermodynamics. The Study of Biochemical Processes at Equilibrium*; Wiley: Chichester, 1983; pp 165−169.

ATP.[3] It is reasonable to assume that the activation barrier for the direct **14** → **11** path in solution is no higher than that measured from the Arrhenius plot for the overall process **15** → **11**, i.e., that both pathways have a low barrier in aqueous solution.

To rationalize the occurrence of the two competing pathways in the overall reaction of **6**−**9** (Scheme 2) and the contrary position with **10**, which appears to react only by a single pathway (the non-methyl analogue of the route via **16** and **17**), it was necessary to consider the additional factor of flux through different intermediates. The study by Schwörer and Wirz[4b] explains the kinetics of acid-catalyzed decay of *aci*-nitro anions of the type considered here, i.e., that cyclization to a benzisoxazoline such as **17** requires prior protonation of the *aci*-nitro anion and is therefore controlled by the p*K* of this species. The decay of **15** is considerably faster than that of its nonmethylated analogue, which indicates that **15** is the stronger base of the two compounds. The underlying reasons for this difference in basicity and its consequences are discussed below.

aci-Nitro anions of type **15** are expected to be stronger bases than the corresponding species lacking the α-methyl substituent, because of the combined actions of the inductive effect of the methyl group and poorer solvation of the more substituted system. A stereoelectronic factor probably also operates to destabilize **15** relative to its nonmethylated analogue. Our gas-phase PM3 calculations showed a dihedral angle between the exocyclic C−C and C−N bonds in **15** of 42.6° for the *Z*-configuration shown (calculated for the species derived from **6** with its carboxylate group in an ionized state; note that calculations for the *E*-configuration gave a similar dihedral angle). By contrast in the non-methyl analogue of **15**, where the alkoxy substituent has a preferred *E*-configuration that minimizes steric crowding (i.e., structure **22**), this dihedral angle was calculated to be 2.5° (cf. calculations by Dunkin et al.[19] for different isomers of the nitronic acid derived from 2-nitrobenzyl methyl ether, which consistently show a planar conformation for the *E*-configuration but twisting of ∼30° for the *Z*-configuration). To test the effects of this twisting, semiempirical calculations that include solvation effects were carried out using the AMSOL program.[22,23] Solvation energies were calculated for the deprotonation reaction of the respective nitronic acid isomers derived from **6** and **10**, respectively, to their corresponding *aci*-nitro anions. These energy differences calculated for the deprotonation reaction (**14** → **15**) showed that the *aci*-nitro anion derived from **10** is 15 kJ mol^{-1} better stabilized than the anion from **6**, which corresponds to a difference of at least 2.6 pK_a units between the two nitronic acids; that is, the nitronic acid derived from **10** is significantly more acidic than that derived from **6** (and by extension from **7**−**9**).

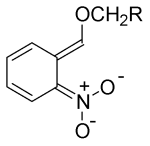

22

From these data it appears reasonable in the methyl-substituted series, where the initial nitronic acid **14** is of substantially weaker acidity than the corresponding species that lacks the α-methyl group, that the rearrangement of **14** that leads directly to the hemiacetal **11** could be in competition with the alternative of ionization to the *aci*-nitro anion **15**. Once ionization has occurred, the *aci*-nitro anion will be kinetically trapped, with its decay controlled by the second-order rate constant for reprotonation. The protonation step is more likely to take place on the less-hindered oxygen to give **16**, followed by cyclization to **17**. For the nitronic acid of higher acidity formed initially in the nonmethylated series, ionization is likely to compete more effectively with the direct rearrangement path, so the reaction proceeds entirely (subject to the limits of detectability) via the "conventional" benzisoxazoline route.

The discussion above gives a broad rationale for the reactivity of the compounds investigated here. Further detailed studies beyond the capability of our present instrumentation will be required to delineate details of individual steps. The present work however does highlight the likely importance of differing acidities of structurally diverse nitronic acids that has not previously been considered.

Conclusions

The overall results of this study and the proposal outlined above to explain the kinetic records of Figure 2 obtained upon flash photolysis of **9** have general implications for the field of caged compounds. A particularly significant point for their use in time-resolved biological studies is that reliance solely on *aci*-nitro decay rates can be misleading as an indicator of the rate of product release. Our data demonstrate that the discrepancy can in some cases be very large and reinforce the value of complementary time-resolved infrared measurements to study this photochemistry. The elegant work by Toscano and colleagues[24] on photochemistry of diazeniumdiolates further shows the value of the technique in unraveling mechanistic details of dark reactions triggered by photolysis. Indeed, it is noteworthy that they were also able to detect two competing mechanistic pathways in their study.

The duality of mechanism uncovered in our work is interesting, as it requires competition between very rapid alternative pathways. From the discussion presented here, this partition appears to be controlled by the pK_a of the initially formed nitronic acid, but it is of interest that the participation of dual pathways has not previously been observed in *o*-nitrobenzyl photocleavage reactions. In cases such as caged ATP, it seems likely that the presence of an anionic side chain very near the nitro group would facilitate ionization of the initial nitronic acid (analogous to **14**), thereby channeling the reaction via the slower *aci*-nitro path. Nevertheless, we recognize that our analysis leaves questions open. For example, the fact that the partitioning between fast and slow processes for photolysis of **6**−**9** is independent of pH (as judged by the pH-invariant amplitude of the 406 nm transients for **9**) suggests that additional considerations may be relevant, in particular the extent to which partitioning of **14** is influenced by reaction from a vibrationally excited state. The factors that promote formation of a hemiacetal

(22) Hawkins, G. D.; Giesen, D. J.; Lynch, G. C.; Chambers, C. C.; Rossi, I.; Storer, J. W.; Li, J.; Zhu, T.; Rinaldi, D.; Liotard, D. A.; Cramer, C. J.; Truhlar, D. G. *AMSOL* version 6.5.3; University of Minnesota: Minneapolis, 1997.
(23) Cramer, C. J.; Truhlar, D. G. *J. Comput. Chem.* **1992**, *13*, 1089.
(24) Srinivasan, A.; Kebede, N.; Saavedra, J. E.; Nikolaitchik, A. V.; Brady, D. A.; Yourd, E.; Davies, K. M.; Keefer, L. K.; Toscano, J. P. *J. Am. Chem. Soc.* **2001**, *123*, 5465.

intermediate in the photolysis of **6**−**9** but not for the nor-analogue **10** also remain to be explored. We hope the data presented here will stimulate further enquiry into this mechanistically diverse area.

Experimental Section

General and Spectroscopic Details. Details of the preparation of compounds **6**−**10** and **12** and of the product study and quantum yield determination for photolysis of **9** are given as Supporting Information. Note that both 2-methyl-2-(2-nitrophenyl)-1,3-dioxolane (the starting material for preparation of **6**−**10**) and **12** are compounds previously described but were prepared here by modified, more satisfactory procedures, as described in the Supporting Information. The time-resolved IR spectrometer was as described previously,[8] and IR measurements were performed in buffers made by adjusting 200 mM solutions of 2-(*N*-morpholino)ethanesulfonic acid (MES), 3-(*N*-morpholino)propanesulfonic acid (MOPS), *N*-(2-hydroxyethyl)piperazine-*N*′-3-propanesulfonic acid (EPPS), Bicine, 2-(*N*-cyclohexylamino)-ethanesulfonic acid (CHES), or 3-(*N*-cyclohexylamino)propanesulfonic acid (CAPS) with 3 M NaOH to pH values specified in the text. To analyze the kinetics of carbonyl formation and nitroso monomer decay for compounds **6**−**9**, we averaged the kinetic difference spectra from three separate samples of each compound and integrated the appropriate bands. Integration was performed using Bruker Opus NT 3D 3.1 software with respect to a baseline drawn between two data points of the spectrum at each side of the band. The two baseline points were calculated by averaging data points in a specified spectral range. Spectral ranges for calculating the two baseline points and for the integration were 1665−1674 and 1706−1734 cm^{-1} (baseline points) and 1679−1694 cm^{-1} (carbonyl band) and 1477−1489 and 1512−1523 cm^{-1} (baseline points) and 1494−1508 cm^{-1} (nitroso band), respectively. The data were analyzed as single-exponential functions by least-squares fits in Microsoft Excel.

The time-resolved UV−visible spectrometer was as previously described[2] except that photolysis was triggered by 347 nm light from a frequency-doubled ruby laser (Lumonics QSR2/6, Rugby, U.K.), pulse width ∼30 ns. Separate photomultiplier tubes were used for measurements at 740 nm and for measurements in the range 406−577 nm, as previously described.[2] The cuvette had 4 mm optical paths for both the laser pulse and the probe light. Data were collected on a TDS 210 oscilloscope (Tektronix Inc., Beverton, OR) and transferred to a PC using the Tektronix Wavestar software. Buffer solutions were prepared by pH adjustment with dilute NaOH of appropriate molarity solutions of salts specified in figure captions. Records for measurements at 406 or 577 nm were processed by averaging 2−4 individual traces (uncorrected for blanks) and fitted to single-exponential functions in Microsoft Excel. The 740 nm records were averaged from 16 individual traces and were corrected by subtraction of an averaged equal number of blank traces (obtained from a solution containing the same buffer but without the relevant photolabile compound) to compensate for flash artifacts before fitting the slow component of the trace.

Computational Methods. Semiempirical PM3 calculations were performed using the program package VAMP Version 6.5[25] with the PM3 Hamiltonian.[17] The molecules investigated were energetically optimized to a gradient norm below 0.4 kJ mol^{-1} $Å^{-1}$ using the Eigenvector Following (EF) algorithm.[25] In the reaction path calculations a step width of 0.05 Å was used. Geometries of transition states were taken from the points on the reaction path calculations that showed a maximum in energy. Subsequent transition state searches showed that the resulting energies are within 0.4 kJ mol^{-1} of those taken from the reaction path calculations and are thus well within the error limit of the underlying method. Calculations that included solvation effects were carried out with the AMSOL program[22] using the default settings along with the PM3-SM3 Hamiltonian.[23]

Acknowledgment. We are grateful to Professor Werner Mäntele for provision of facilities, to the Royal Society for an ESEP grant that facilitated collaboration between the U.K. and German laboratories, and to the MRC Biomedical NMR Centre for access to NMR instrumentation. We also thank the EPSRC National Mass Spectrometry Centre for negative ion mass spectrometric measurements.

Supporting Information Available: Sources or synthetic procedures and characterization for compounds **6**−**10** and **12**, quantum yield determination, and product study for photolysis of **9** (PDF). This material is available free of charge via the Internet at http://pubs.acs.org.

JA034354C

(25) Rauhut, G.; Alex, A.; Chandrasekhar, J.; Steinke, T.; Sauer, W.; Beck, B.; Hutter, M.; Gedeck, P.; Clark, T. *VAMP* Version 6.5; Oxford Molecular: Erlangen, 1997.